Azimuth ambiguity elimination for borehole imaging using 3D borehole RTM scheme

Junxiao Li, Kris Innanen, Guo Tao, Laurence R. Lines and Kuo Zhang

ABSTRACT

The azimuth ambiguity has been an issue ever since the beginning of borehole acoustic reflection imaging. The reason of this imaging authenticity indistinguishability occurring not only in the borehole reflection imaging but also in seismic imaging is due to the intrinsic defect of the 2D data processing that treats recorded real data as a 2D data set, which inevitably leads us to take for granted that the data (which actually may be from every possible direction of underneath formations) is only from one direction. The 4-C dipole acoustic well logging technique is then applied to solve the azimuth ambiguity problem by analyzing the azimuthal information contained in the recorded shear wave signals. Thereafter, the migration procedure is carried out to get the imaging result. In this paper, the 3D reverse time migration in the borehole environment is proposed and applied in the simulated data set with a similar source and receiver system as sonic scanner tool developed by Schlumberger. The result shows the directional information of the structures outside the borehole can be directly obtained.

INTRODUCTION

The image of geological structures away from the borehole can be acquired by analyzing recorded data from borehole acoustic measurements by applying seismic imaging schemes (Hornby, 1989; Li et al., 2002). Monopole acoustic imaging has produced positive results in delineating near borehole structures (Fortin et al., 1991; Coates et al., 2000; Li et al., 2002). One of the flaws of the omni-directional monopole acoustic prototype is it only measures the acoustic pressure and is therefore insensitive to determine the reflector azimuth.

In order to mitigate this directional ambiguity, the dipole acoustic reflection imaging is developed (Tang et al., 2003; Tang, 2004; Tang and Patterson, 2009; Bolshakov et al., 2011). In dipole methods, dispersive flexure waves, whose velocity at the cutoff frequency equals the S-wave velocity, are analyzed.these data, given the deviation angle of the well bore and the tool azimuthal angle, can determine the azimuth of the structures outside the borehole after migration (Tang et al., 2003). Tang (Tang et al., 2007) applied this technique to dipole S-wave log data. He also developed a method to extract the shear wave reflection signals which were then used to get the S-wave imaging.

Besides the inspiring results from the dipole acoustic reflection imaging, Li (Li et al., 2014a) applied the blind signal separation method into the synthetic horizontal data from Sonic scanner tool to get the separated reflections from different reflectors. However, the amplitude information can not be conserved by using this method. Rougha (Al Rougha et al., 2005), Yamamoto (Yamamoto et al., 2000) and Haldorsen (Haldorsen et al., 2006) developed a 3D assembly of hydrophones on the logging tool, where 4 or 8 omnidirectional hydrophones are located azimuthally around the tool (Sonic Scanner tool developed

by Schlumberger), trying to get azimuthal information from hydrophones towards different directions. However, the migration and imaging results provided by this tool are independently obtained by 2D seismic processing techniques from different evenly spaced receivers (Haldorsen et al., 2010; Li et al., 2013). Reverse time migration (RTM) is not a new seismic prestack depth migration method, which was first introduced in the late 1970s (Hemon, 1978)and shows promising imaging capabilities (Baysal et al., 1983; Whitmore et al., 1983; McMechan, 1983; Loewenthal and Mufti, 1983). Because of its expensive computational cost, the three dimensional (3-D) prestack RTM is yet available until recent years (Yoon et al., 2003). In the application of borehole acoustic reflection imaging, the 2-D borehole RTM in isotropic medium is first introduced in 2014 (Li et al., 2014b).

In this paper, we first simulate the recorded waveforms of the 8 evenly spaced hydrophones using a staggered-grid finite difference method. And then a 3-D RTM in borehole environment is developed and thus used for migration of the reflection signals extracted from the simulated waveforms. To make a comparison, the 2-D synthetic data of two horizontal wells is also simulated and migrated by a 2-D borehole RTM scheme.

THEORY AND PRINCIPLES OVERVIEW

The basic theory of RTM is simple, which mainly is composed of simulation of source wavefield, backward simulation of the received waveforms and the application of imaging condition, where, the forward and backward wavefield simulation are realized by the staggered-grid finite difference (FD) method in this paper. For details of elastic wave equation using FD method in VTI medium in this paper, let's begin with the velocity-stress equation in elastic medium, in which the Hook's law states,

$$\sigma_{ij,j} = c_{ijkl}\varepsilon_{kl} \tag{1}$$

where c_{ijkl} are the elastic constants, and the strain tensor ε_{kl} is defined as,

$$\varepsilon_{kl} = \frac{1}{2}(u_{k,l} + u_{l,k}) \tag{2}$$

The matrix form of equation (1) can be described as,

$$\begin{bmatrix}\sigma_{11}\\ \sigma_{22}\\ \sigma_{33}\\ \sigma_{23}\\ \sigma_{23}\\ \sigma_{12}\end{bmatrix} = \begin{bmatrix}c_{11} & c_{12} & c_{13} & c_{14} & c_{15} & c_{16}\\ c_{21} & c_{22} & c_{23} & c_{24} & c_{25} & c_{26}\\ c_{31} & c_{32} & c_{33} & c_{34} & c_{35} & c_{36}\\ c_{41} & c_{42} & c_{43} & c_{44} & c_{45} & c_{46}\\ c_{51} & c_{52} & c_{53} & c_{54} & c_{55} & c_{16}\\ c_{61} & c_{62} & c_{63} & c_{64} & c_{65} & c_{66}\end{bmatrix} \begin{bmatrix}\varepsilon_{11}\\ \varepsilon_{22}\\ \varepsilon_{33}\\ 2\varepsilon_{23}\\ 2\varepsilon_{13}\\ 2\varepsilon_{12}\end{bmatrix} \tag{3}$$

In the above equation, the elastic constant tensor in a vertical transverse isotropic medium (VTI) can be described as,

$$c_{VTI} = \begin{bmatrix} c_{11} & c_{11}-2c_{66} & c_{13} & 0 & 0 & 0\\ c_{11}-2c_{66} & c_{11} & c_{13} & 0 & 0 & 0\\ c_{13} & c_{13} & c_{33} & 0 & 0 & 0\\ 0 & 0 & 0 & c_{44} & 0 & 0\\ 0 & 0 & 0 & 0 & c_{44} & 0\\ 0 & 0 & 0 & 0 & 0 & c_{66}\end{bmatrix} \tag{4}$$

Based on the above equations, the first order velocity and stress equations can be described as,

$$\begin{aligned}
\frac{\partial \sigma_{xx}}{\partial x} + \frac{\partial \sigma_{xy}}{\partial y} + \frac{\partial \sigma_{xz}}{\partial z} &= \rho \frac{\partial V_x}{\partial t} \\
\frac{\partial \sigma_{yx}}{\partial x} + \frac{\partial \sigma_{yy}}{\partial y} + \frac{\partial \sigma_{yz}}{\partial z} &= \rho \frac{\partial V_y}{\partial t} \\
\frac{\partial \sigma_{zx}}{\partial x} + \frac{\partial \sigma_{zy}}{\partial y} + \frac{\partial \sigma_{zz}}{\partial z} &= \rho \frac{\partial V_z}{\partial t}
\end{aligned} \tag{5}$$

and,

$$\begin{aligned}
\frac{\partial \sigma_{xx}}{\partial t} &= c_{11} \frac{\partial V_x}{\partial x} + (c_{11} - 2c_{66}) \frac{\partial V_y}{\partial y} + c_{13} \frac{\partial V_z}{\partial z} \\
\frac{\partial \sigma_{yy}}{\partial t} &= (c_{11} - 2c_{66}) \frac{\partial V_x}{\partial x} + c_{11} \frac{\partial V_y}{\partial y} + c_{13} \frac{\partial V_z}{\partial z} \\
\frac{\partial \sigma_{zz}}{\partial t} &= c_{13} \frac{\partial V_x}{\partial x} + c_{13} \frac{\partial V_y}{\partial y} + c_{33} \frac{\partial V_z}{\partial z} \\
\frac{\partial \sigma_{yz}}{\partial t} &= c_{44} (\frac{\partial V_y}{\partial z} + \frac{\partial V_z}{\partial y}) \\
\frac{\partial \sigma_{xz}}{\partial t} &= c_{44} (\frac{\partial V_x}{\partial z} + \frac{\partial V_z}{\partial x}) \\
\frac{\partial \sigma_{xy}}{\partial t} &= c_{66} (\frac{\partial V_x}{\partial y} + \frac{\partial V_y}{\partial x})
\end{aligned} \tag{6}$$

where (V_x, V_y, V_z) is the velocity vector. Based on the staggered-grid FD method(Virieux, 1986), equation (5) can be written as,

$$\begin{aligned}
V_x^{n+\frac{1}{2}} &= V_x^{n-\frac{1}{2}} + \frac{\Delta t}{\rho} (\delta_x \sigma_{xx}^n + \delta_y \sigma_{xy}^n + \delta_z \sigma_{xz}^n) \\
V_y^{n+\frac{1}{2}} &= V_y^{n-\frac{1}{2}} + \frac{\Delta t}{\rho} (\delta_x \sigma_{xy}^n + \delta_y \sigma_{yy}^n + \delta_z \sigma_{yz}^n) \\
V_z^{n+\frac{1}{2}} &= V_z^{n-\frac{1}{2}} + \frac{\Delta t}{\rho} (\delta_x \sigma_{xz}^n + \delta_y \sigma_{yz}^n + \delta_z \sigma_{zz}^n)
\end{aligned} \tag{7}$$

where, we take $\delta_x \sigma_{xx}^n$ as an example,

$$\delta_x \sigma_{xx}^n (l_x + \frac{1}{2}, l_y, l_z) = \frac{1}{\Delta x} \sum_{m=0}^{N-1} a_m [\sigma_{xx}^n (l_x + m + 1, l_y, l_z) - \sigma_{xx}^n (l_x + m, l_y, l_z)] \tag{8}$$

Likewise, equation (6) can be discretized as,

$$\begin{aligned}
\sigma_{xx}^{n+1} &= \sigma_{xx}^{n} + \Delta t[c_{11}\delta_x V_x^{n+1/2} + (c_{11}-2c_{66})\delta_y V_y^{n+1/2} + c_{13}\delta_z V_z^{n+1/2}] \\
\sigma_{yy}^{n+1} &= \sigma_{yy}^{n} + \Delta t[(c_{11}-2c_{66})\delta_x V_x^{n+1/2} + c_{11}\delta_y V_y^{n+1/2} + c_{13}\delta_z V_z^{n+1/2}] \\
\sigma_{zz}^{n+1} &= \sigma_{zz}^{n} + \Delta t[c_{13}\delta_x V_x^{n+1/2} + c_{13}\delta_y V_y^{n+1/2} + c_{33}\delta_z V_z^{n+1/2}] \\
\sigma_{yz}^{n+1} &= \sigma_{yz}^{n} + \Delta t c_{44}[\delta_y V_z^{n+1/2} + \delta_z V_y^{n+1/2}] \\
\sigma_{xz}^{n+1} &= \sigma_{xz}^{n} + \Delta t c_{44}[\delta_x V_z^{n+1/2} + \delta_z V_x^{n+1/2}] \\
\sigma_{xy}^{n+1} &= \sigma_{xy}^{n} + \Delta t c_{66}[\delta_x V_y^{n+1/2} + \delta_y V_x^{n+1/2}]
\end{aligned} \tag{9}$$

The forward wavefield propagation can thus be simulated by the above equations with a source term added in the normal stress terms. For a dipole source simulation, we put two monopole- sources with opposite phase close to the borehole wall. Being symmetric to the center of the borehole, the two monopole- sources are designated on a specified coordinate axis(x- or y- axis). Likewise, the backward wavefield simulation can also be obtained by a similar scheme, except equation (7) and equation (9) should be written as,

$$\begin{aligned}
V_x^{n-\frac{1}{2}} &= V_x^{n+\frac{1}{2}} - \tfrac{\Delta t}{\rho}(\delta_x \sigma_{xx}^{n} + \delta_y \sigma_{xy}^{n} + \delta_z \sigma_{xz}^{n}) \\
V_y^{n-\frac{1}{2}} &= V_y^{n+\frac{1}{2}} - \tfrac{\Delta t}{\rho}(\delta_x \sigma_{xy}^{n} + \delta_y \sigma_{yy}^{n} + \delta_z \sigma_{yz}^{n}) \\
V_z^{n-\frac{1}{2}} &= V_z^{n+\frac{1}{2}} - \tfrac{\Delta t}{\rho}(\delta_x \sigma_{xz}^{n} + \delta_y \sigma_{yz}^{n} + \delta_z \sigma_{zz}^{n})
\end{aligned} \tag{10}$$

and,

$$\begin{aligned}
\sigma_{xx}^{n} &= \sigma_{xx}^{n+1} - \Delta t[c_{11}\delta_x V_x^{n+1/2} + (c_{11}-2c_{66})\delta_y V_y^{n+1/2} + c_{13}\delta_z V_z^{n+1/2}] \\
\sigma_{yy}^{n} &= \sigma_{yy}^{n+1} - \Delta t[(c_{11}-2c_{66})\delta_x V_x^{n+1/2} + c_{11}\delta_y V_y^{n+1/2} + c_{13}\delta_z V_z^{n+1/2}] \\
\sigma_{zz}^{n} &= \sigma_{zz}^{n+1} - \Delta t[c_{13}\delta_x V_x^{n+1/2} + c_{13}\delta_y V_y^{n+1/2} + c_{33}\delta_z V_z^{n+1/2}] \\
\sigma_{yz}^{n} &= \sigma_{yz}^{n+1} - \Delta t c_{44}[\delta_y V_z^{n+1/2} + \delta_z V_y^{n+1/2}] \\
\sigma_{xz}^{n} &= \sigma_{xz}^{n+1} - \Delta t c_{44}[\delta_x V_z^{n+1/2} + \delta_z V_x^{n+1/2}] \\
\sigma_{xy}^{n} &= \sigma_{xy}^{n+1} - \Delta t c_{66}[\delta_x V_y^{n+1/2} + \delta_y V_x^{n+1/2}]
\end{aligned} \tag{11}$$

And the received reflections are treated as source signals added in the normal stress terms. For the imaging condition, the normalized imaging condition (Cogan et al., 2011)

is used in this paper to eliminate the unwanted noise. And after the superposition of the imaging result of each shot, the Laplacian filter is also applied to mitigate the low frequency noise.

SIMULATION AND COMPARISON WITH 2D BOREHOLE RTM

In this section, the 2D synthetic data sets are first analyzed to reveal the problem of azimuth detection ambiguity. The model of the 2D synthetic data is set to be a horizontal well, where a borehole horizontally locates in the middle. And then a 3D synthetic model with two interfaces parallel to a vertical borehole are simulated. The strikes of the two interfaces stretch towards y axis (Figure 7).

As we can see from Figure 1, a well filled with water horizontally penetrates into a fast formation (formation in red, with its Vp and Vs being 4000 m/s, 2300 m/s, respectively). The influence of the sonic tool is also taken into consideration in this model, where we set the Vp and Vs velocity and the density of the tool as 5860 m/s, 3300 m/s, 7850 kg/m^3, respectively. An interface with a dip angle of 15° on the top of the model (formation in chartreuse, with its Vp and Vs being 3000 m/s, 1800 m/s, respectively). Let the sonic tool move from left to right at a starting poing of (x=2 m, z=6 m) and set the distance from the source to the first receiver as 3.27 m, with two arrays (each array has 13 hydrophones with a spacing of 0.15 m) of receivers sitting on both sides of the borehole wall. A data set of all together 40 shots is thus generated with a total recording time of 0.01 s (recording time sample is $5e-7$ s).

Figure 2 shows reflection signals of the synthetic model. Figure 2 (a) shows reflections recorded by the upper array of receivers, whereas, Figure 2 (b) shows reflections from the lower array of receivers (the energy of reflection signal in (b) is multiplied by 5). As we can see, although the interface is on the upper layer of the model and the existence of the borehole fluid and acoustic tool acts as blocks preventing the reflections from the upper interface being received by the lower array of the receivers, however, there is still considerable reflection energy received by the lower receivers, which will inevitably play a negative influence on the imaging result. As a result, only the reflections from the upper layer are used to the next migration step. The imaging result is shown in Figure 5. Unfortunately, because of the intrinsically azimuthal ambiguity in 2D environment, the borehole RTM cannot tell which side the reflections are coming from and there is no way but to focus the reflection energy on both sides of the borehole, which in tern, produces a counterfeit reflector lying symmetrically with the true interface.

Figure 3 shows a similar geometrical model with Figure 1, except there is another dip interface (with a dip angle of 15°) below the horizontal well. The parameters of formations for the upper and middle layers are the same with those in Figure 1. The Vp and Vs velocities in the lower layer are 4500 m/s, 2600 m/s respectively. The borehole radiation mechanisms and reception response (source, receiver arrays and the correspondent parameters such as offset and receivers spacing) are the same with the previous model. Figure 4 shows the reflection signals of the synthetic model. Figure 4 (a) shows reflections recorded by the upper array of receivers, whereas, Figure 4 (b) shows reflections from the lower array of receivers (the energy of reflection signal in (b) is multiplied by 5). Because of

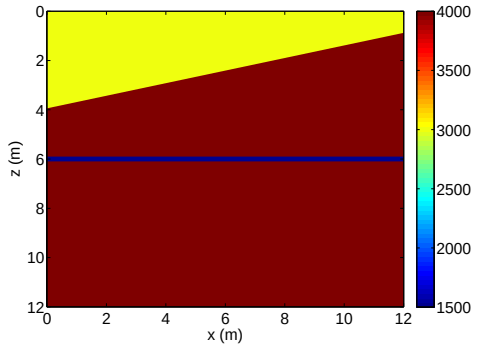

FIG. 1. The synthetic model of a horizontal well filled with water (blue) horizontally penetrates into a fast formation (red). A dip interface locates on the top of the model.

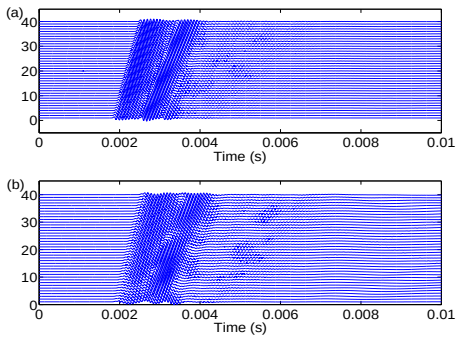

FIG. 2. The reflection signals of the synthetic model: (a) The reflections recorded by the upper array of receivers; (b) the reflections from the lower array of receivers.

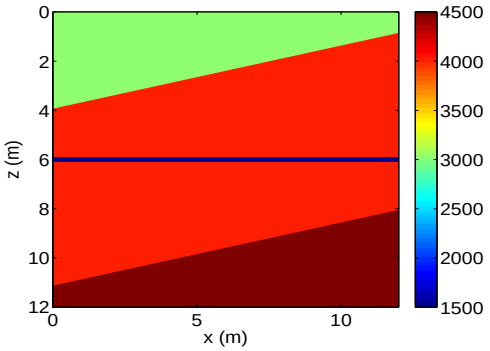

FIG. 3. The synthetic model of a horizontal well filled with water (blue) horizontally penetrates into a fast formation (red).

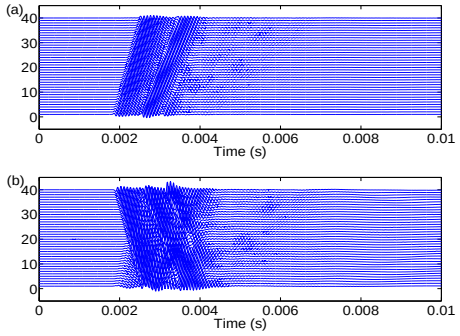

FIG. 4. The reflection signals of the synthetic model:The reflections recorded by the upper array of receivers (a) and lower array of receivers (b).

the difference of the geometrical distribution of the two interfaces, the reflection energy received by the lower array of receivers is smaller than that received by the upper ones. Nevertheless, we should note from the picture that the lower receivers can still receive the reflection signals from the upper interface. The imaging result is shown in Figure 6. The two interfaces from each side of the borehole are now distributed on both sides.

Although Tang (Tang, 2004) successfully calculated the strike of the reflector outside the borehole using the shear wave directional information. This technique is only available in the presence of a dipole source. Wang (Wang et al., 2015) found the arrival times of reflections in different azimuth receivers of the monopole tool are different, based on which, he successfully determined the strike of the reflector. In this paper, we want to provide a much more intuitionistic way to solve the azimuthal ambiguity by applying a 3D borehole RTM into the reflections recorded by 8 omnidirectional hydrophones located azimuthally around the tool.

As we can see in Figure 7, the formation between the two reflectors is a slow VTI formation whose elastic parameters are,

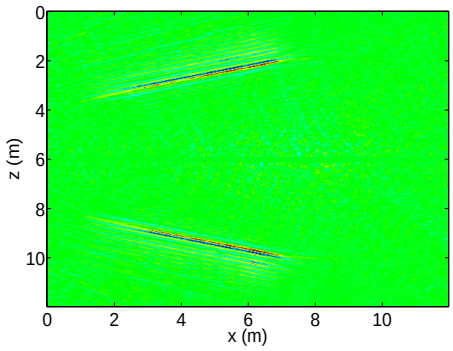

FIG. 5. Imaging result of the upper interface model.

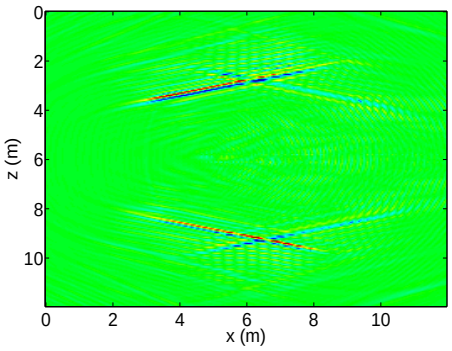

FIG. 6. Imaging result of the model with interfaces on both sides of the well.

$$c_{VTI} = \begin{bmatrix} 23.87 & 15.33 & 9.79 & 0 & 0 & 0 \\ 15.33 & 23.87 & 9.79 & 0 & 0 & 0 \\ 9.79 & 9.79 & 15.33 & 0 & 0 & 0 \\ 0 & 0 & 0 & 2.77 & 0 & 0 \\ 0 & 0 & 0 & 0 & 2.77 & 0 \\ 0 & 0 & 0 & 0 & 0 & 4.27 \end{bmatrix} \tag{12}$$

The interface in brown is 2 m away from the well, whereas the interface in gray on the other side is 2.5 m away from the borehole. Formations outside the two interfaces are isotropic media (Vp=4000 m/s, Vs=2300 m/s). A dipole source with a central frequency of 2000 Hz emits energy towards x axis. The 8 receiver arrays are evenly spaced around the well, with 20 hydrophones in each array. The distance between the nearest hydrophone to the dipole source is 1 m and the hydrophone spacing of each array is 0.15 m. The total recording time is 1 ms with a time sample of 5 μs. Figure 8 shows a cross-section profile of the 3D model in x-z plane. Following the work flow proposed by Li (Li et al., 2014b), Figure 9 shows the snapshots of the forward wavefield propagation in x-z plane from borehole fluid to the formation outside the borehole with the time increasing from 1.5 ms to 5.25 ms. It is apparent from the snapshots that when the wavefield propagates to the interfaces, the reflections on both sides of the borehole are generated and bounce back from the interfaces to the borehole. The arrival time of the reflections on both sides to the borehole is different because of the different distances of the interfaces from the borehhole. The imaging result for one shot of the 3D model are then shown in Figure 10, where we can see that, the two interfaces are focused in the right locations (the one in the left side denotes the horizontal cross section of the brown interface in Figure 7. The center of the well is in position (x=80, z), with a H-PML layer (Zhang et al., 2014) of 15 grids outside each surface of the model, the distance between left reflector to the center of the well is 40 grids or 2 m; the reflector on the right side is 50 grids or 2.5 m away from the borehole.), which solves the azimuthal ambiguity of the 2D method we discussed before.

To make a comparison, a monopole source is applied in the next synthetic model, where 8 receiver arrays are evenly spaced around the well, with 20 hydrophones in each array. As we can see in Figure 11, an interface in brown is 2 m away from the well with a strike

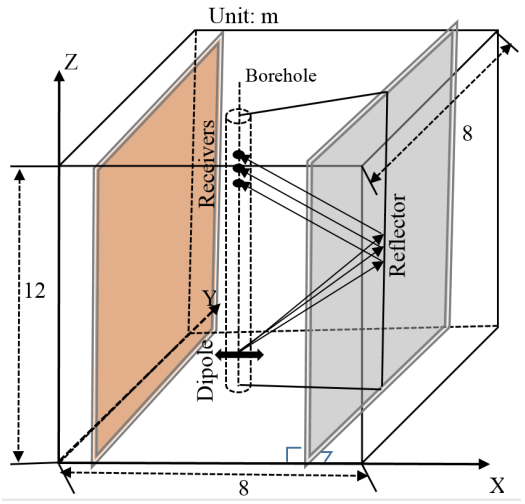

FIG. 7. The 3D profile of the VTI model with a dipole source and 8 evenly spaced hydrophones.

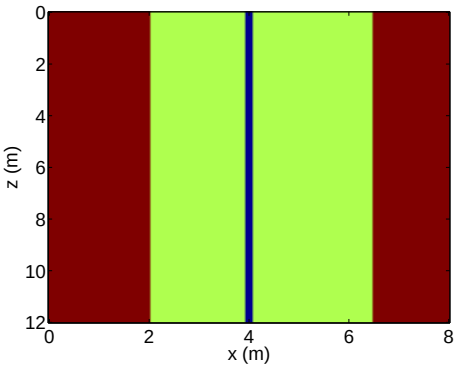

FIG. 8. A cross-section profile of the 3D model in x-z plane.

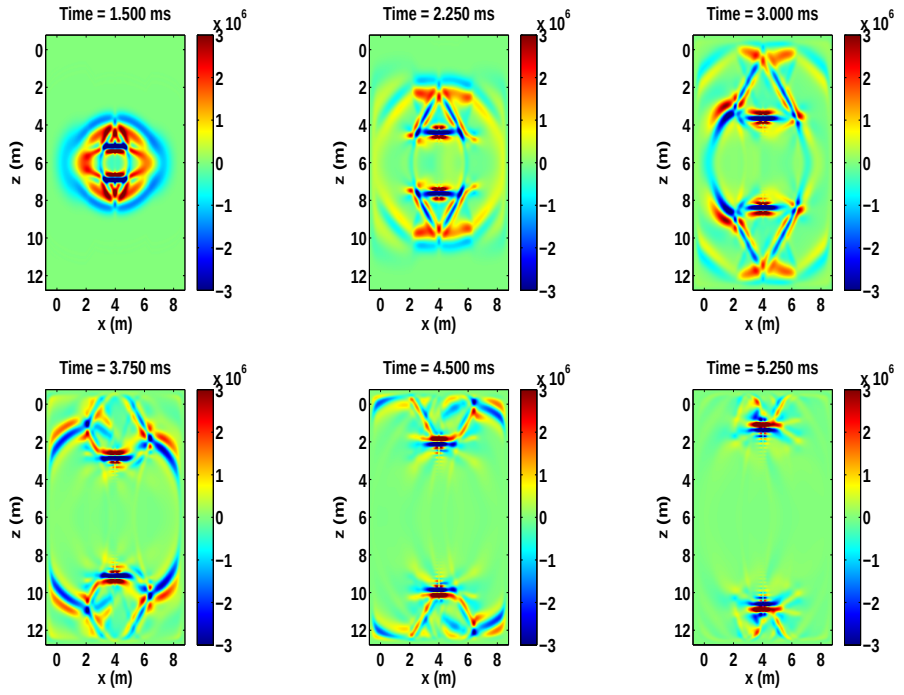

FIG. 9. The snapshots of the forward wavefield propagation in x-z plane from borehole fluid to the formation outside the borehole with the time increasing from 1.5 ms to 5.25 ms.

perpendicular to x axis, whereas the interface in gray on the other side has a strike of 45° from the borehole. The elastic parameters of the formations outside the borehole are the same with those in previous model. To have a better geometrical understanding, Figure 12 also shows a cross-section profile of the 3D model in x-z plane. The distance between the nearest hydrophone to the monopole source is 1 m and the hydrophone spacing of each

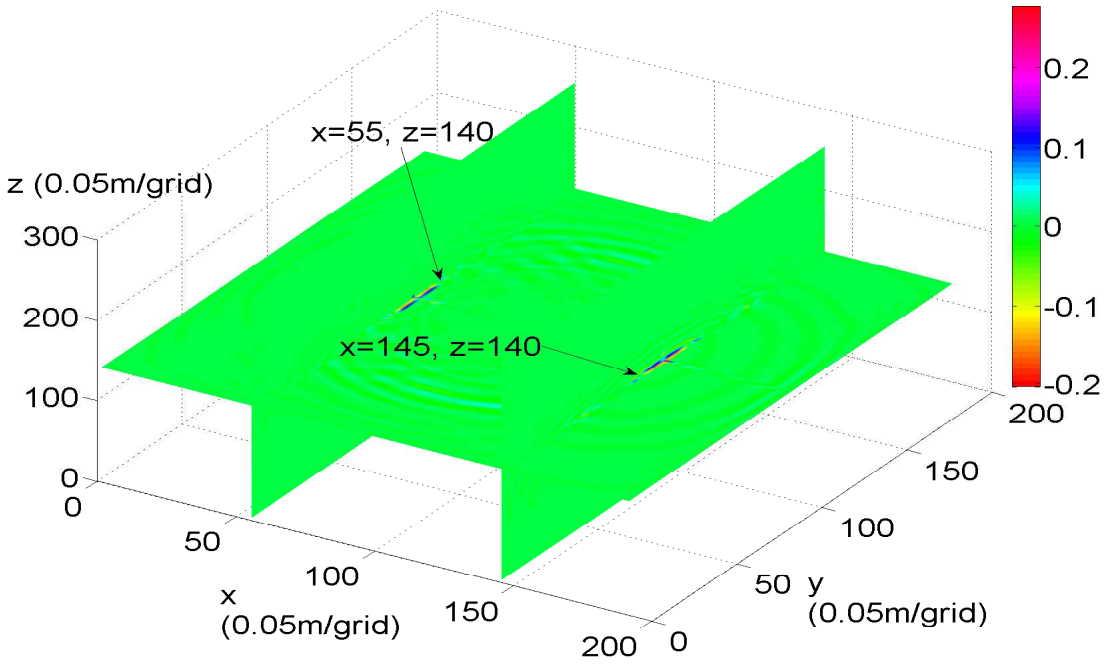

FIG. 10. The imaging result for one shot of the 3D model.

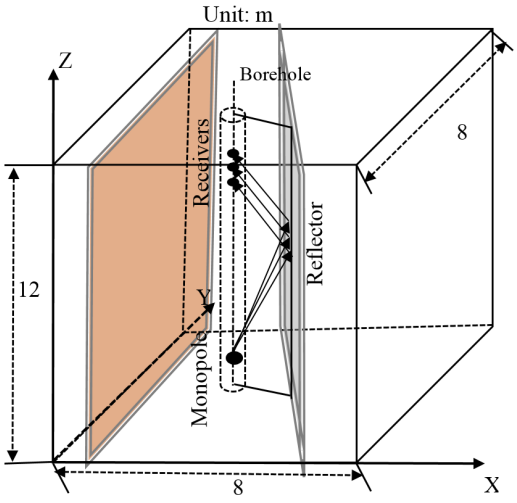

FIG. 11. The 3D profile of the VTI model with a monopole source and 8 evenly spaced hydrophones.

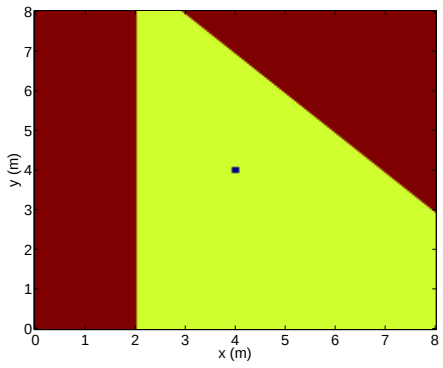

FIG. 12. A cross-section profile of the 3D model in x-z plane.

array is 0.15 m. The imaging result for all together 15 shots of the 3D model are then shown in Figure 13, where we can see that, the two interfaces are also focused in the right locations, which demonstrates the 3D borehole RTM can solve the azimuthal ambiguity even with a monopole source.

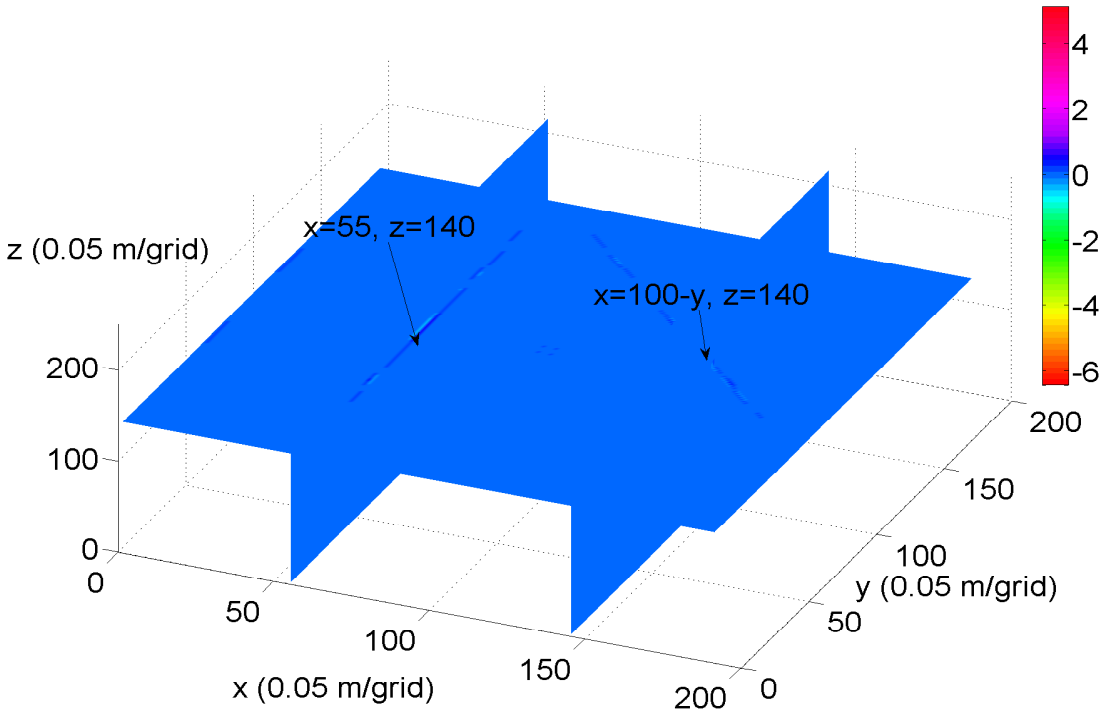

FIG. 13. The imaging result for one shot of the 3D model.

CONCLUSIONS

Most of the methods and principles for borehole acoustic reflection imaging, to date, are mainly applied in a 2D environment. The distance and dip angles of the structures such as vugs and fractures outside a borehole can then be delineated by means of borehole migration and imaging technique. To our disappointment however, one of the issues is that, the azimuth information for the structures away from the borehole can hardly be acquired due to the mechanism of borehole radiation and reception response per se.

In this paper, the two horizontal models illustrate the generation of azimuthal ambiguity in imaging. And the 3D borehole RTM is proposed in this paper to solve the azimuth ambiguity problem, taking the advantage of 8 omnidirectional hydrophones evenly spaced around the borehole to receive reflections from all directions. The imaging results of the 3D synthetic model show the azimuthal ambiguity problem can be fixed even with a monopole source.

ACKNOWLEDGMENTS

The authors thank the sponsors of CREWES for continued support. This work was funded by CREWES industrial sponsors and NSERC (Natural Science and Engineering Research Council of Canada) through the grant CRDPJ 461179-13. Author 1 was also supported by SEG scholarship and Shell.

REFERENCES

Al Rougha, H., Sultan, A., Haldorsen, J. et al., 2005, Integration of microelectrical and sonic reflection imaging around the borehole-offshore uae: SPE, **11021**.

Baysal, E., Kosloff, D. D., and Sherwood, J. W., 1983, Reverse time migration: Geophysics, **48**, No. 11, 1514–1524.

Bolshakov, A. O., Patterson, D. J., Lan, C. et al., 2011, Deep fracture imaging around the wellbore using dipole acoustic logging, *in* SPE Annual Technical Conference and Exhibition, Society of Petroleum Engineers.

Coates, R., Kane, M., Chang, C., Esmersoy, C., Fukuhara, M., Yamamoto, H. et al., 2000, Single-well sonic imaging: High-definition reservoir cross-sections from horizontal wells, *in* SPE/CIM International Conference on Horizontal Well Technology, Society of Petroleum Engineers.

Cogan, M., Fletcher, R., King, R., Nichols, D. et al., 2011, Normalization strategies for reverse-time migration, *in* 2011 SEG Annual Meeting, Society of Exploration Geophysicists.

Fortin, J., Rehbinder, N., Staron, P. et al., 1991, Reflection imaging around a well with the eva full-waveform tool: The Log Analyst, **32**, No. 03.

Haldorsen, J., Voskamp, A., Thorsen, R., Vissapragada, B., Williams, S., Fejerskov, M. et al., 2006, Borehole acoustic reflection survey for high resolution imaging, *in* 2006 SEG Annual Meeting, Society of Exploration Geophysicists.

Haldorsen, J. B., Zhu, F., Hirabyashi, N., Borland, W. H., Kurniawan, H., Yamamoto, H., Al-Ghammari, K., and Coates, R., 2010, Borehole acoustic reflection survey (bars) using full waveform sonic data: first break, **28**.

Hemon, C., 1978, Equations d'onde et modeles*: Geophysical Prospecting, **26**, No. 4, 790–821.

Hornby, B. E., 1989, Imaging of near-borehole structure using full-waveform sonic data: Geophysics, **54**, No. 6, 747–757.

Li, J., Tao, G., Zhang, K., and Liu, H., 2014a, Acoustic reflection signals extraction by applying blind signal separation, *in* 76th EAGE Conference and Exhibition 2014.

Li, J., Tao, G., Zhang, K., Wang, B., and Wang, H., 2014b, An effective data processing flow for the acoustic reflection image logging: Geophysical Prospecting, **62**, No. 3, 530–539.

Li, J., Tao, G., Zhang, K., Yel, Q. et al., 2013, Borehole sonic reflection imaging by finite difference reverse time migration, *in* 2013 SEG Annual Meeting, Society of Exploration Geophysicists.

Li, Y., Zhou, R., Tang, X., Jackson, J., and Patterson, D., 2002, Single-well imaging with acoustic reflection survey at mounds, oklahoma, usa, *in* 64th EAGE Conference & Exhibition.

Loewenthal, D., and Mufti, I. R., 1983, Reversed time migration in spatial frequency domain: Geophysics, **48**, No. 5, 627–635.

McMechan, G. A., 1983, Seismic tomography in boreholes: Geophysical Journal International, **74**, No. 2, 601–612.

Tang, X., Dubinsky, V., Harrison, C. et al., 2003, Logging-while-drilling shear and compressional measurements: case histories, *in* SPWLA 44th Annual Logging Symposium Transactions.

Tang, X., Zheng, Y., and Patterson, D., 2007, Processing array acoustic-logging data to image near-borehole geologic structures: Geophysics, **72**, No. 2, E87–E97.

Tang, X. M., 2004, Imaging near-borehole structure using directional acoustic-wave measurement: Geophysics, **69**, No. 6, 1378–1386.

Tang, X.-M., and Patterson, D. J., 2009, Single-well s-wave imaging using multicomponent dipole acoustic-log data: Geophysics, **74**, No. 6, WCA211–WCA223.

Virieux, J., 1986, P-sv wave propagation in heterogeneous media: Velocity-stress finite-difference method: Geophysics, **51**, No. 4, 889–901.

Wang, H., Tao, G. et al., 2015, A method to determine the strike of interface outside of borehole by monopole borehole acoustic reflections: Journal of Petroleum Science and Engineering, **133**, 304–312.

Whitmore, N. et al., 1983, Iterative depth migration by backward time propagation, *in* 1983 SEG Annual Meeting, Society of Exploration Geophysicists.

Yamamoto, H., Watanabe, S., Koelman, J., Geel, J., Brie, A., Fujii, K., Coates, R. et al., 2000, Borehole acoustic reflection survey experiments in horizontal wells for accurate well positioning, *in* SPE/CIM International Conference on Horizontal Well Technology, Society of Petroleum Engineers.

Yoon, K., Shin, C., Suh, S., Lines, L. R., and Hong, S., 2003, 3d reverse-time migration using the acoustic wave equation: An experience with the seg/eage data set: The Leading Edge, **22**, No. 1, 38–41.

Zhang, K., Tao, G., Li, J., Wang, H., Liu, H., and Ye, Q., 2014, 3d fdm modeling of acoustic reflection logging in a deviated well, *in* 76th EAGE Conference and Exhibition 2014.